energies

IMPACT FACTOR 3.0

CITESCORE 6.2

Article

Modeling and Control of Ejector-Based Hydrogen Circulation System for Proton Exchange Membrane Fuel Cell Systems

Zecheng Xu, Bo Liu, Yuqi Tong, Zuomin Dong and Yanbiao Feng

MDPI

https://doi.org/10.3390/en17112460

energies

MDPI

Article

Modeling and Control of Ejector-Based Hydrogen Circulation System for Proton Exchange Membrane Fuel Cell Systems

Zecheng Xu [1], Bo Liu [1], Yuqi Tong [2], Zuomin Dong [3] and Yanbiao Feng [1,3,*]

[1] School of Mechanical Engineering, University of Science and Technology Beijing, Beijing 100083, China; xzcxzcxzc123456@126.com (Z.X.); liubo1@ustb.edu.cn (B.L.)
[2] State-Assigned Electric Vehicle Power Battery Testing Center, China North Vehicle Research Institute, Beijing 100072, China
[3] Department of Mechanical Engineering and Institute for Integrated Energy Systems, University of Victoria, Victoria, BC V8W 2Y2, Canada
* Correspondence: yfeng@ustb.edu.cn

Abstract: Ejector-based proton exchange membrane fuel cells (PEMFCs) are of great interest due to their simplicity and feasibility. Thus, proton exchange membrane fuel cells are considered the most suitable technology for in-vehicle systems, industrial applications, etc. Despite the passive characteristics of the ejector, active control of the hydrogen supply system is needed to ensure sufficient hydrogen, maintain the stack pressure, and ensure effective entrainment. In this research, a novel semi-empirical model is proposed to accurately predict the entrainment performance of the ejector with an 80 kW fuel cell system. According to the precise semi-empirical model, the hydrogen supply system and the anode channel are modeled. Then, a fuzzy logic controller (FLC) is developed to supply sufficient and adequate gas flow and maintain the rapid dynamic response. Compared to the conventional proportional–integral–derivative controller, the fuzzy logic controller could reduce the anode pressure variability by 5% during a stepped case and 2% during a dynamic case.

Keywords: hydrogen circulation system; ejector-based circulation; ejector semi-empirical modeling; proton exchange membrane fuel cell system; fuzzy logic control; PID control

Citation: Xu, Z.; Liu, B.; Tong, Y.; Dong, Z.; Feng, Y. Modeling and Control of Ejector-Based Hydrogen Circulation System for Proton Exchange Membrane Fuel Cell Systems. *Energies* **2024**, *17*, 2460. https://doi.org/10.3390/en17112460

Academic Editor: Giovanni Esposito

Received: 16 April 2024
Revised: 12 May 2024
Accepted: 17 May 2024
Published: 21 May 2024

1. Introduction

As the global economy rapidly grows, energy demand and usage are rising worldwide, causing traditional energy reserves to fall short of demand [1]. This reliance on conventional energy leads to significant pollution, harming the environment and biodiversity and posing health risks to humans and other organisms. To address these challenges, nations and regions are increasingly recognizing the importance of sustainable development, prioritizing environmental protection, and promoting resource recycling and utilization [2]. The focus on clean, green energy sources is becoming a central theme of the modern era.

As a clean energy carrier, hydrogen has promising potential to reduce greenhouse gas emissions [3]. The PEMFC is a crucial device that converts the hydrogen's chemical energy into electric energy. Being capable of operating efficiently and quietly, refueling fast, and emitting zero carbon oxides, the PEMFC has carved out a niche in the transportation area, especially in long-haul heavy-duty trucks [4–6]. Many fuel cells connected in series comprise the PEMFC stack, which requires accessory systems, including hydrogen supply systems, air supply systems, water-heat management systems, and other electric accessory systems, to ensure efficient and stable operation [7]. Providing the fuel cell stack with steady pressure and fuel, the hydrogen supply system can be categorized according to anodic recirculation forms: an ejector-based, pump-based, and compound recirculation system [8]. Conventional hydrogen recycling methods rely on compressors or circulation pumps to recycle excess hydrogen. However, these methods consume more auxiliary power, lower the fuel cell efficiency, and produce mechanical vibration and noise. In contrast,

the ejector utilizes the pressure difference to recycle hydrogen without additional power consumption. It has a simple structure, low noise, and ease of maintenance, making it an ideal device for recycling hydrogen. Furthermore, incorporating an ejector can also enhance the performance of the fuel cell [9]. Nevertheless, the ejector is a passive device and cannot actively regulate fuel flow. Therefore, fuel flow is usually handled by controlling the opening of the injector valve. Thus, the structure and controller design of the hydrogen supply system are of great significance in improving the performance of the PEMFC [10].

Much research has been carried out to optimize the structure of hydrogen ejectors. Zhu et al. [11] proposed a shock circle model to predict the performance of the newly designed ejector. Dadvar et al. [12] proposed a method that provides an optimal basis for selecting and developing the ejector. Wang et al. [13] carried out the computational fluid dynamics (CFD) calculation and conducted a one-dimensional numeric analysis of ejector performance. Huang et al. [14] developed a one-dimensional model, verified by experiment using R141b as the working fluid. Most studies implement theoretical calculations using thermodynamics and heat and mass transfer theory. Despite the theoretical model being able to be implemented efficiently, the model's accuracy could be improved. The simulation model based on the CFD method can be much more accurate than the theoretical method. Nikiforow et al. [15] modeled an ejector with CFD assuming 2D axisymmetric flow and with three turbulence models. Chen et al. [16] optimized the key geometrical parameters, such as the nozzle diameters of the big nozzle (BN) and small nozzle (SN), as well as the axial distance between the two nozzles through CFD simulation. Han et al. [17] developed a three-dimensional multicomponent CFD model to investigate the synergistic transient characteristics of the hydrogen recirculation components (hydrogen injector, ejector, and purge valve) in an 80 kW PEMFC. However, CFD is time-consuming and cannot be implemented in real-time control.

Control and optimization are required to realize the achievable performance of the optimal design of the ejector as well. He et al. [18] designed a decentralized proportional–integral (PI) controller that dynamically controls the recirculation flow rate while maintaining the anode supply pressure variation and a multivariable linear controller [19] that shows better performance in tracking and immunity. Wang et al. [20] combined the advantages of robust control and PID control to develop a robust PID controller for the PEMFC system. Xue et al. [21] proposed a fuzzy logic PI control method for the hydrogen supply subsystem of a proton exchange membrane fuel cell and used an improved quantum particle swarm optimization method to optimize the controller parameters. Wang et al. [22] developed three control methods, including PID, fuzzy PID control, and PID coupled with model predictive control (PID-MPC), to address the response hysteresis issue. Li et al. [23] used model feedforward combined with PID feedback control methods to achieve dynamic decoupling of the fuel cell hydrogen system and precise control of the hydrogen flow, pressure, and hydrogen permeation ratio. Huang et al. [24] established a new quasi-two-dimensional ejector model by considering the flow phenomena of the boundary layer, shock train, and mixing layer. Yet, much research has been carried out to optimize the performance of ejectors from a structure design and control point of view. There are still challenges and research gaps: the ejector model used in control optimization needs to be more accurate, and the control method should be optimized.

This study aims to model and control the hydrogen supply system to fill the knowledge gap of the ejector-based hydrogen system. The main contributions to the research field are the following.

(1) A semi-empirical model is proposed to predict the ejector's performance accurately.
(2) The developed fuzzy logic controller regulates the anode pressure and hydrogen supply.

To complete the modeling and control of the PEMFC system, we proposed a novel ejector modeling method. Based on this novel ejector model, the complete hydrogen circulation system model was established. Then, a fuzzy controller was developed. Finally, the simulation results revealed the efficacy of the novel ejector model and the fuzzy controller.

2. Materials and Methods

The working principle of the hydrogen cycle system of a PEMFC with an ejector is shown in Figure 1. Ejector-based hydrogen supply systems typically include a hydrogen source, pressure regulator, injector, supply manifold, ejector, electric stack anode, and purge valve [25]. The high-pressure hydrogen is regulated to low-pressure hydrogen and injected into the primary chamber of the ejector. The primary flow entrains the unreacted gas mixture from the anode (secondary flow) in the suction chamber. The two flows are fully expanded in the constant area chamber and then discharged from the diffusion chamber into the anode. Without loss of generality, the following assumptions are made to simplify the model:

1. The hydrogen source outlet pressure is always stable.
2. There is no pressure drop at the piping connections.
3. The variation in space in the gas supply manifold is ignored.
4. The ideal gas law applies to all volumes.

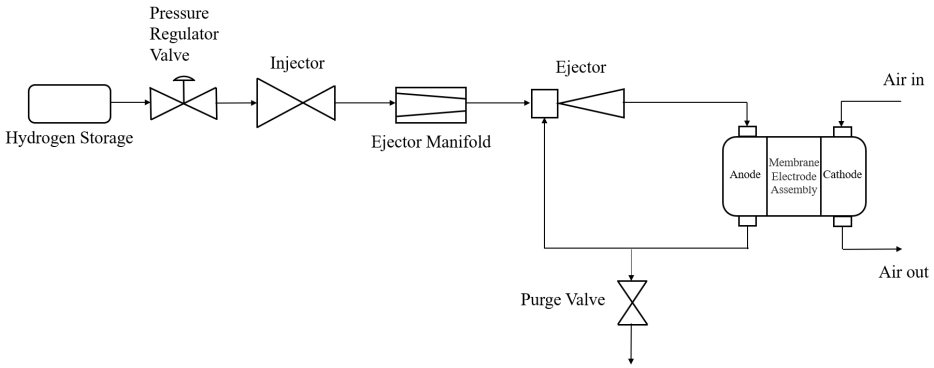

Figure 1. A hydrogen fuel delivery system.

2.1. Injector

In this research, the injector valve is a physical throttle [25], considering both subsonic ($P_{sm}/P_{tank} \geq \gamma_{cr}$) and sonic flow ($P_{sm}/P_{tank} < \gamma_{cr}$). The critical pressure ratio is defined in Equation (1).

$$\gamma_{cr} = \left(\frac{2}{\gamma+1}\right)^{\frac{\gamma}{\gamma-1}} \tag{1}$$

where γ is the specific heat capacity ratio of hydrogen, as defined in Equation (2).

$$\gamma = \frac{C_{p\_H}}{C_{v\_H}} \tag{2}$$

where C_{p_H} (unit, J/(kg·K)) is hydrogen's pressure-specific heat capacity, and C_{v_H} (unit, J/(kg·K)) is hydrogen's volume-specific heat capacity.

The injector mass flow rate $\dot{m}_{inj}$ can be calculated in Equation (3) [25].

$$\dot{m}_{inj} = \begin{cases} A_{inj} \times P_{tank} \times C_{d,inj} \times \sqrt{\frac{2\times\gamma\times(\frac{P_{sm}}{P_{tank}})^{\frac{2}{\gamma}}\times(\frac{P_{sm}}{P_{tank}})^{\frac{\gamma+1}{\gamma}}}{R\times T_{tank}\times(\gamma-1)}}, \frac{P_{sm}}{P_{tank}} \geq (\frac{2}{\gamma+1})^{\frac{\gamma}{\gamma-1}} \\ A_{inj} \times P_{tank} \times C_{d,inj} \times \sqrt{\frac{\gamma}{R\times T_{tank}}\times(\frac{2}{\gamma+1})^{\frac{\gamma+1}{\gamma-1}}}, \frac{P_{sm}}{P_{tank}} < (\frac{2}{\gamma+1})^{\frac{\gamma}{\gamma-1}} \end{cases} \tag{3}$$

where A_{inj} (unit, m^2), P_{tank} (unit, Pa), P_{sm} (unit, Pa), $C_{d,inj}$, T_{tank} (unit, K), and R (unit, J/(mol·K)) are the injector cross-sectional area, pressure regulator valve pressure, supply manifold pressure, non-uniform flow coefficient, hydrogen cylinder temperature, and ideal gas constant, respectively.

2.2. Manifold

The ejector supply manifold connects the injector to the ejector. It is modeled using the ideal gas equation of state and the law of conservation of mass. Equation (4) describes the dynamic gas pressure model of the manifold.

$$\frac{dP_{sm}}{dt} = \frac{R \times T_{sm}}{V_{sm}} \times (\dot{m}_{sm,in} - \dot{m}_{sm,out}) \tag{4}$$

T_{sm} (unit, K) is the supply manifold temperature, and V_{sm} (unit, m^3) is the supply manifold volume. $\dot{m}_{sm,in}$ (unit, kg/s) and $\dot{m}_{sm,out}$ (unit, kg/s) are the mass flow rates of the input and output pipes, respectively.

2.3. Ejector

The ejector is structurally composed of a suction chamber, a constant area chamber, and a diffuser. The primary flow input to the ejector is pure hydrogen. The secondary flow is the circulation gas from the anode, a mixture of hydrogen, nitrogen, and vapor. Two flows are mixed inside the ejector and discharged through the diffusion chamber. Figure 2 depicts the schematic diagram of the ejector.

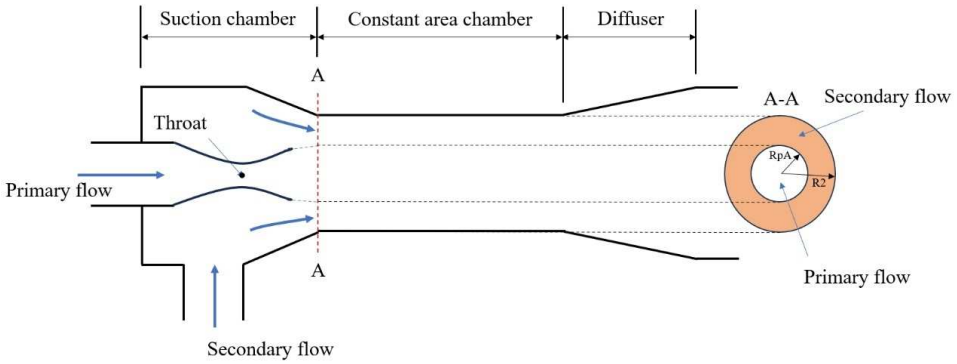

Figure 2. Schematic of ejector.

According to the pressure ratio of primary and secondary flow (P_{sec}/P_{pri}), the ejector's working state can be categorized into choking and non-choking. If $P_{sec}/P_{pri} \geq V_{CR}$, the ejector is non-choking. The primary flow properties, including mass flow rate $\dot{m}_{pri}$ (unit, kg/s), velocity V_{priA} (unit, m/s), and Mach number M_{priA}, can be obtained in Equations (5)–(7).

$$\dot{m}_{pri} = P_{pri} \times A_{throat} \times \sqrt{\frac{2 \times \varphi_p \times \gamma \times ((\frac{P_{sec}}{P_{pri}})^{\frac{2}{\gamma}} - (\frac{P_{sec}}{P_{pri}})^{\frac{\gamma+1}{\gamma}})}{(\gamma - 1) \times R \times T_{pri}}} \tag{5}$$

$$V_p = \sqrt{(1 - (\frac{P_{sec}}{P_{p_{ri}}})^{\frac{\gamma-1}{\gamma}}) \times C_{p\_H} \times 1000 \times 2 \times T_{p_{ri}}} \tag{6}$$

$$M_{priA} = \frac{V_{priA}}{\sqrt{2 \times \frac{\gamma}{\gamma+1}} \times 500 \times R \times T_{pri}} \tag{7}$$

where P_{pri} (unit, Pa) is the primary flow pressure, A_{throat} (unit, m^2) is the ejector throat cross-sectional area, φ_p is the isentropic flow coefficient, T_{pri} (unit, K) is the primary flow temperature, and D_{throat} (unit, m) is the diameter of the ejector throat.

The diameter of the primary flow in the non-choking state at the A-A cross-section (D_{pA}) is equal to the diameter of the ejector's throat, D_{throat}.

$$D_{pA} = D_{throat} \tag{8}$$

When $P_{sec}/P_{pri} < V_{CR}$, the ejector is operated in the choking state. The primary flow properties are calculated using Equations (9)–(11).

$$\dot{m}_{pri} = P_{pri} \times A_{throat} \times \sqrt{\frac{\varphi_p}{(R \times T_{pri})} \times \frac{2}{\gamma+1}^{\frac{\gamma+1}{2(\gamma-1)}}} \tag{9}$$

$$M_{pA} = \sqrt{\frac{2 \times ((\frac{P_{pri}}{P_{sec}})^{\frac{\gamma-1}{\gamma}} - 1)}{\gamma - 1}} \tag{10}$$

$$V_p = M_{pA} \times \sqrt{2 \times T_{pri} \times R \times \frac{\gamma}{({M_{pA}}^2 \times (\gamma-1)+2)}} \tag{11}$$

The effective diameter of the expanded primary flow D_{priA} is estimated by Equation (12).

$$D_{priA} = \frac{((\gamma-1) \times {M_{pA}}^2 + 2) \times D_{throat} \times \sqrt{\frac{1}{M_{pA}}}}{((\gamma-1) \times {M_t}^2 + 2)^{\frac{\gamma+1}{4(\gamma-1)}} \times \sqrt{P_{pri\_psi} \times P_{sec\_psi}}} \tag{12}$$

where M_t is the flow Mach number at the shock circle, P_{pri_psi} (unit, bar) is the primary flow pressure. P_{sec_psi} (unit, bar) is the secondary flow pressure.

To model the entrained flow, this research assumed that the primary flow is fully expanded in the constant area chamber, forming an A-A cross-section with a circular working cross-section, shown in Figure 2. The cylindrical area of the primary flow created an annular flow cavity, bounded by the physical inner wall of the ejector constant chamber. A pressure difference was imagined at the annular flow cavity on the left and right sides of the A-A section. The imaginary pressure difference enforced the secondary flow. This pressure difference was related to the Mach number of the primary flow at section A-A, the diameter of the constant area chamber and throat, etc. It can be obtained by data fitting, such as polymer curve fitting, neural network fitting, etc.

$$\Delta P = f(D_{throat}, D_2, M_{priA}, \ldots) \tag{13}$$

where D_2 (unit, m) is the diameter of the constant area chamber.

Thus, the secondary flow rate $\dot{m}_{sec}$ could be obtained from Equation (14).

$$\dot{m}_{sec} = (1 - (1-\Delta P)^{\frac{\gamma-1}{\gamma}}) \times 2 \times \frac{\gamma}{\gamma-1} \times (1-\Delta P)^{\frac{1}{\gamma}} \times \frac{\sqrt{P_{pri\_psi}} \times \frac{\pi}{4} \times ({D_2}^2 - {D_{pA}}^2) \times P_{sec}}{\sqrt{\frac{R \times T_{sec}}{m_{mix}}}} \tag{14}$$

where m_{mix} (unit, kg/mol) is the molar mass of the secondary flow. T_{sec} (unit, K) is the temperature of the secondary flow.

2.4. Anode Channel Modeling

Considering the fuel cell stack's anode channel as a lumped volume, it could be simplified to a capacitive cavity by neglecting gas permeation and liquid water transport across the proton exchange membrane. Hydrogen enters the anode flow channel, where a portion of the hydrogen is consumed to generate electrical energy, and the other portion flows out into the recirculation line. Based on the ideal gas equation of state and mass conservation, the dynamic of the anode pressure is described in Equation (15).

$$\frac{dP_{an}}{dt} = \frac{R \times T_{an}}{V_{an}} \times (\dot{m}_{an,in} - \dot{m}_{an,out} - \dot{m}_{an,reacted}) \tag{15}$$

where P_{an} (unit, Pa) is the anode pressure, T_{an} (unit, K) is the anode temperature of the stack, V_{an} (unit, m^3) is the anode volume of the stack. $\dot{m}_{an,in}$ (unit, kg/s) and $\dot{m}_{an,out}$ (unit, kg/s) is the hydrogen flow rate in and out. $\dot{m}_{an,reacted}$ (unit, kg/s) is the hydrogen flow rate consumed by the anode stack, which is calculated as Equation (16).

$$\dot{m}_{an,reacted} = I_{st} \times \frac{N_{cell} \times m_{H_2}}{2F} \tag{16}$$

where I_{st} (unit, A) is the stack's load current, m_{H_2} (unit, kg/mol) is the molecular weight of hydrogen, N_{cell} is the number of cells, and F (unit, C/mol) is the Faraday constant.

2.5. Purge Valve

The valve model was established from the mass flow equation. The purge valve mass flow rate $\dot{m}_{pur}$ is modeled in Equation (17).

$$\dot{m}_{pur} = \begin{cases} A_{pur} \times P_{an} \times C_{d,pur} \times \sqrt{\frac{2\times\gamma_{mix}}{R\times T_{an}\times(\gamma_{mix}-1)} \times (1-\frac{1}{P_{an}})^{\frac{\gamma_{mix}-1}{\gamma_{mix}}}}, \frac{1}{P_{an}} \geq (\frac{2}{\gamma_{mix}+1})^{\frac{\gamma_{mix}}{\gamma_{mix}-1}} \\ A_{pur} \times P_{an} \times C_{d,pur} \times \sqrt{\frac{\gamma_{mix}}{R\times T_{an}}} \times (\frac{2}{\gamma_{mix}+1})^{\frac{\gamma_{mix}+1}{2(\gamma_{mix}-1)}}, \frac{1}{P_{an}} \geq (\frac{2}{\gamma+1})^{\frac{\gamma_{mix}}{\gamma_{mix}-1}} \end{cases} \tag{17}$$

where A_{pur} (unit, m^2) is the cross-sectional area of the purge valve, $C_{d,pur}$ is the non-uniform flow coefficient, and γ_{mix} is the specific heat capacity ratio of the mixture.

The parameters used for the model construction are given in Table 1.

Table 1. Model parameters.

Parameters	Symbols	Value
Injector cross-sectional area	A_{inj} [25]	3.85×10^{-5} m^2
Pressure regulator valve pressure	P_{tank}	2×10^6 Pa
Non-uniform flow coefficient	$C_{d,inj}$ [25]	0.42
Hydrogen cylinder temperature	T_{tank}	298.15 K
Ideal gas constant	R	8.314 J/(mol·K)
Hydrogen's pressure-specific heat capacity	C_{p_H}	14.05 J/(kg·K)
Hydrogen's volume-specific heat capacity	C_{v_H}	9.934 J/(kg·K)
Area of the ejector's throat	A_{throat} [13]	2.659×10^{-6} m^2
Diameter of the ejector's throat	D_{throat} [13]	1.84×10^{-3} m
Supply manifold volume	V_{sm} [19]	4×10^{-3} m^3
Isentropic flow coefficient	φ_p [12]	0.95
Diameter of constant area chamber	D_2 [13]	5.9×10^{-3} m
Anode volume of the stack	V_{an} [19]	5.3×10^{-3} m^3
Number of cells	N_{cell}	1200

2.6. Model Validation

The ejector entrainment coefficients (ω) were obtained at hydrogen mass flow rates up to 80, 140, 154.8, 180, and 200 PLSM, respectively, and the CFD calculations were obtained from the literature [26]. As shown in Figure 3, the semi-empirical model fitting results were very close to the CFD calculations, and the maximum error occurred at the mass flow rate of 140 PLSM, which was 2.4%. The accuracy of the ejector constructed based on the novel modeling method is verified. The ejector entrainment coefficient is calculated as Equation (18):

$$\omega = \frac{\dot{m}_{sec}}{\dot{m}_{pri}} \tag{18}$$

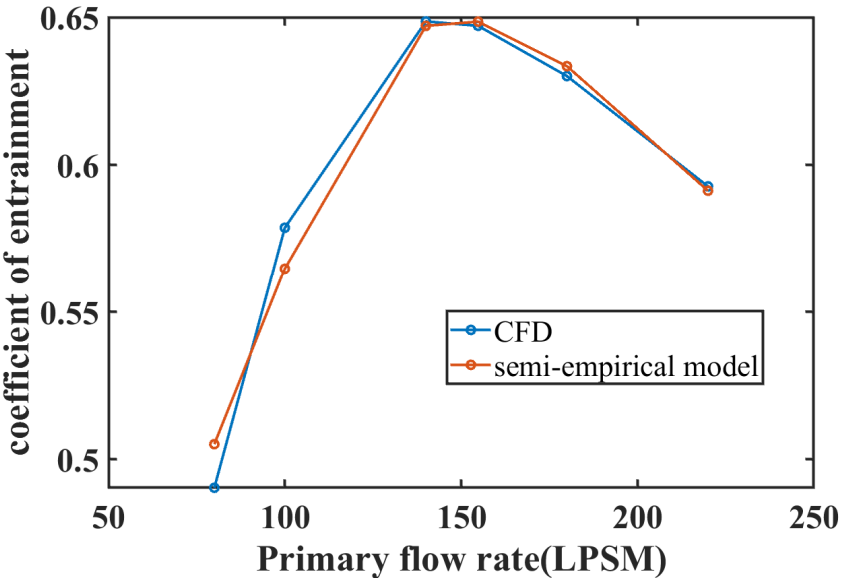

Figure 3. Calculation results of semi-empirical model and CFD.

2.7. Fuzzy Logic Control

Fuzzy logic control (FLC) utilizes fuzzy logic to make decisions and control the controller's output [27]. Fuzzy control consists of five main steps: the definition of input and output variables, fuzzification, design of fuzzy control rules, inference, and defuzzification [28]. The flowchart is shown in Figure 4.

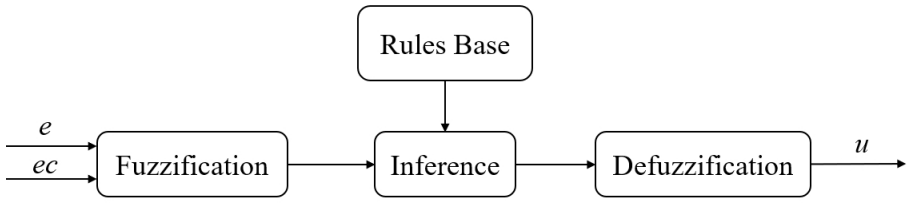

Figure 4. Fuzzy controller flowchart.

The opening of the injector valve was positively correlated with the hydrogen flow rate. In this research, a fuzzy PID control was proposed to regulate the injector's opening, thus altering the hydrogen flow rate and the pressure of the fuel cell stack's anode. Figure 5 illustrates the closed-loop fuzzy PID control system.

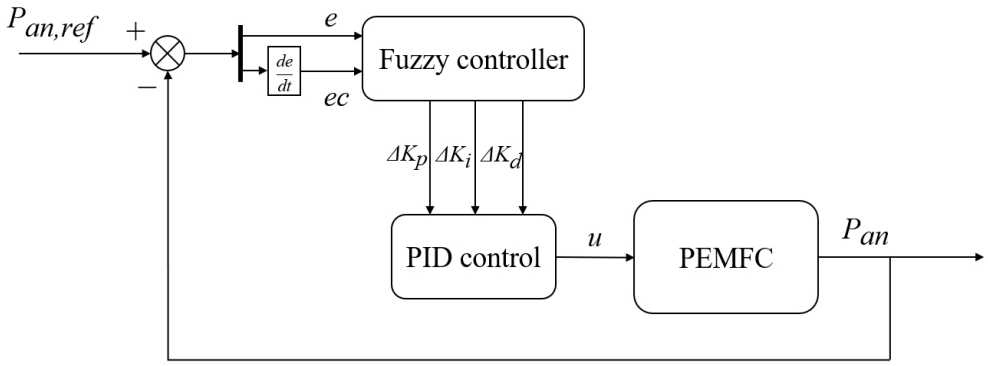

Figure 5. Closed-loop fuzzy control system.

This fuzzy control system regulated the anode pressure using two input signals: the pressure difference in the reference and feedback, marked as $e(t)$, and the change

rate of the pressure difference, observed as $ec(t)$. u is the opening of the injector valve, forming the output of the fuzzy control system. The adaptive proportional, integral, and differential coefficients are denoted as ΔK_p ΔK_i ΔK_d, respectively, which can be obtained via the adaptive results of the fuzzy logic controller. $e(t)$ and $ec(t)$ can be described in Equations (19) and (20).

$$e(t) = P_{an,ref} - P_{an}(t) \tag{19}$$

$$ec(t) = \frac{de(t)}{dt} \tag{20}$$

where $P_{an,ref}$ (unit, Pa)is the anode target pressure, $P_{an}(t)$ (unit, Pa) is the actual pressure.

2.7.1. Fuzzification

Fuzzification converts the deterministic values of the controller inputs to the corresponding values of fuzzy linguistic variables using fuzzy affiliation functions [29]. In this research, the affiliation functions of both input variables were Gaussian type, and the affiliation functions of the three output variables were triangular type. The fuzzy definition domain of all the variables is given in Table 2. K_{p0}, K_{i0}, and K_{d0} scale factors were 0.75, 2.07, and 0.075, respectively.

Table 2. Fuzzy definition domain of all variables.

Parameters	Variables	Fuzzy Definition Domain
Pressure difference	$e(t)$	$(-3, 3)$
Change rate of pressure difference	$ec(t)$	$(-20, 20)$
Adaptive proportional coefficient	ΔK_p	$(-0.05, 0.05)$
Adaptive integral coefficient	ΔK_i	$(-0.1, 0.1)$
Adaptive differential coefficient	ΔK_d	$(-0.01, 0.01)$

2.7.2. Inference Rules

The input and output signals of the fuzzy control system are fuzzy variables assigned to seven linguistic variables, marked as NB (negative large), NM (negative medium), NS (negative small), ZO (zero), PS (positive small), PM (positive medium), and PB (positive large) [30].

If the pressure difference (e) is significant, the value of K_p should be increased to improve the system's response time and quickly reduce the output error. A moderate K_i should be taken, and K_d should be as small as possible. If the pressure difference (e) is average, reducing the value of K_p is necessary to prevent the system from overshooting. Then, the values of K_i and K_d need to be adjusted so that the system is fast and stable simultaneously. If the pressure difference (e) is slight, more consideration should be given to the effect of the changing rate of the pressure difference on the system. When the pressure difference changing rate (ec) is significant, a smaller value of K_d should be used to avoid system oscillations. If the changing rate of the pressure difference (ec) is small, K_d should be more prominent.

Fuzzy inference rules based on the above principles were created and are shown in Tables 3–5.

Table 3. Fuzzy inference rules of ΔK_p.

ΔK_p		*ec*						
		NB	NM	NS	ZO	PS	PM	PB
e	NB	PB	PB	PM	PM	PS	ZO	ZO
	NM	PB	PB	PM	PS	PS	ZO	NS
	NS	PM	PM	PM	PS	ZO	NS	NS
	ZO	PM	PM	PS	ZO	NS	NM	NM
	PS	PS	PS	ZO	NS	NS	NM	NB
	PM	PS	ZO	NS	NM	NM	NM	NB
	PB	ZO	ZO	NM	NM	NM	NB	NB

Table 4. Fuzzy inference rules of ΔK_i.

ΔK_i		*ec*						
		NB	NM	NS	ZO	PS	PM	PB
e	NB	NB	NB	NM	NM	NS	ZO	ZO
	NM	NB	NB	NM	NS	NS	ZO	ZO
	NS	NB	NM	NS	NS	ZO	PS	PS
	ZO	NM	NM	NS	ZO	PS	PM	PM
	PS	NM	NS	ZO	PS	PS	PM	PB
	PM	ZO	ZO	PS	PS	PM	PB	PB
	PB	ZO	ZO	PS	PM	PM	PB	PB

Table 5. Fuzzy inference rules of ΔK_d.

ΔK_d		*ec*						
		NB	NM	NS	ZO	PS	PM	PB
e	NB	PS	NS	NB	NB	NB	NM	PS
	NM	PB	NS	NB	NM	NM	NS	ZO
	NS	ZO	NS	NM	NM	NS	NS	ZO
	ZO	ZO	NS	NS	NS	NS	NS	ZO
	PS	ZO	ZO	ZO	ZO	ZO	ZO	ZO
	PM	PB	PS	PS	PS	PS	PS	PB
	PB	PB	PM	PM	PM	PS	PS	PB

2.7.3. Inference Engine

Fuzzy inference is a language that describes inference using fuzzy inference rules based on fuzzy judgments. A fuzzy inference engine is an operational method that formulates logical decisions and transforms the fuzzy rules into fuzzy language and outputs. In this paper, the Mamdani fuzzy inference method is used. The adaptive proportional, integral, and differential coefficients of the inference surface are shown in Figure 6.

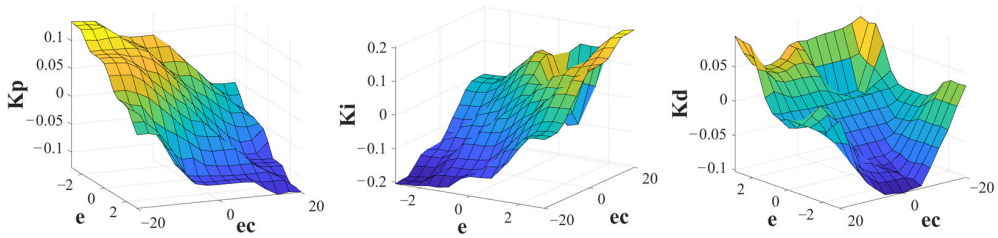

Figure 6. The inference surface.

2.7.4. Defuzzification

The defuzzification is needed to translate the fuzzy PID parameters into accurate values. This paper uses the center of gravity method for defuzzification. The output variable can be described as Equation (21).

$$u = \frac{\sum_{i=1}^{n} u_i A(u_i)}{\sum_{i=1}^{n} A(u_i)} \tag{21}$$

where u is the exact value of the output variable, u_i is the fuzzy value of the output variable, and $A(u_i)$ is the affiliation function.

3. Results

Simulations under two typical cases were carried out to verify the effectiveness of the proposed fuzzy controller. First, the fuel cells' current steps from 200 A to 300 A (given by Figure 7a), which simulate the instant high-power demand corresponding to the fuel cell electric vehicle suddenly accelerating from cruise speed. Then, a dynamic case contains multiple ascending and descending steps in the current (shown in Figure 8a), which can simulate the fuel cell vehicle's continuous acceleration and deceleration. The parameters of the conventional PID controller used as a comparison are K_p = 0.38, K_i = 0.9, and K_d = 0.05. The simulation was carried out on the MATLAB/Simulink platform.

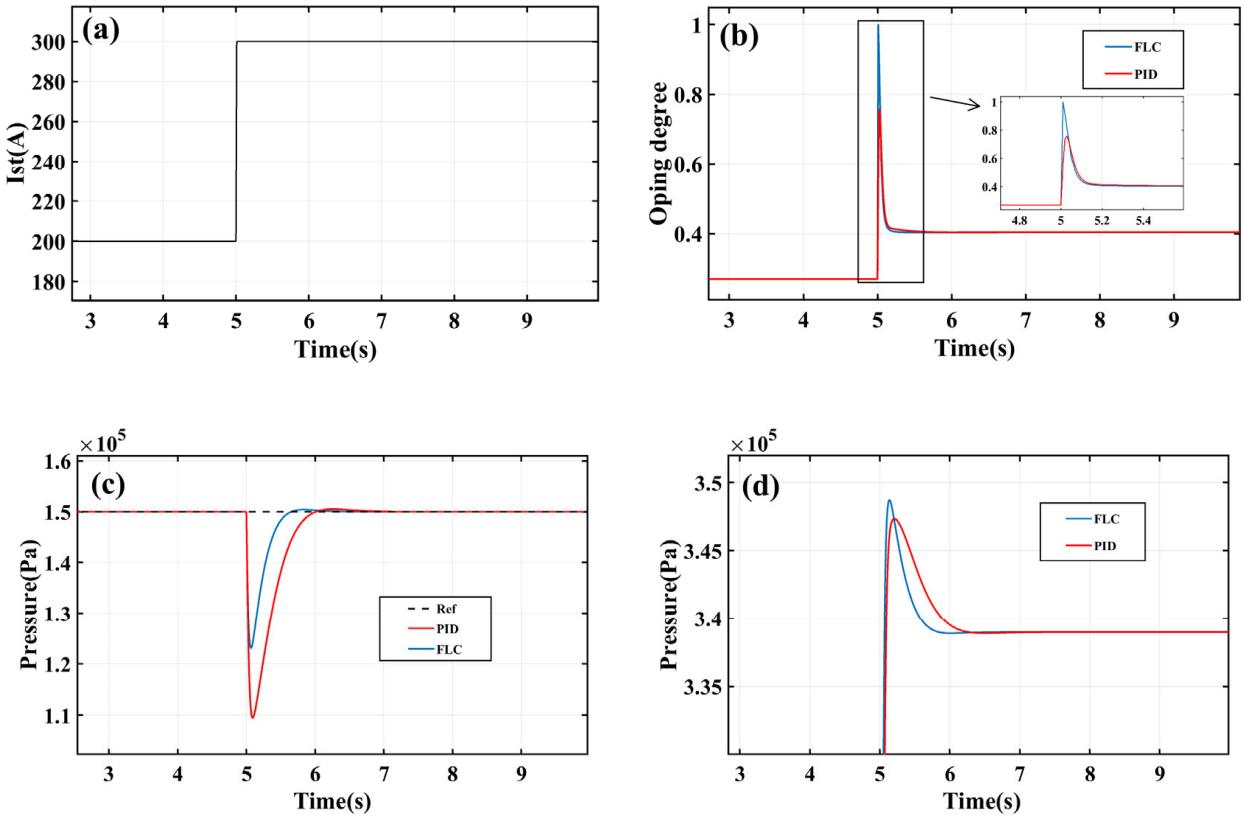

Figure 7. (**a**) Fuel cell stack current; (**b**) injector valve opening; (**c**) anode pressure; (**d**) supply manifold pressure.

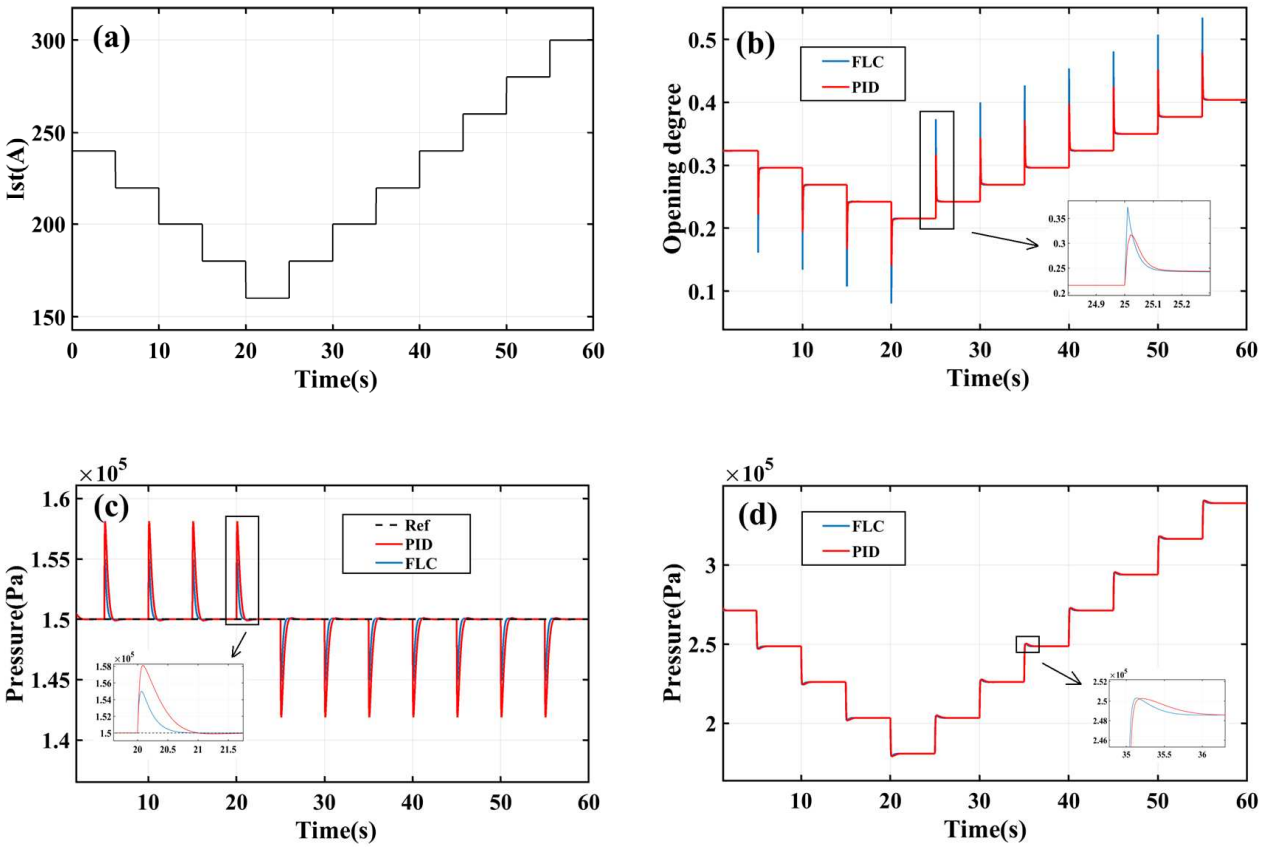

Figure 8. (**a**) Fuel cell stack current; (**b**) injector valve opening; (**c**) anode pressure; (**d**) supply manifold pressure.

3.1. Performance under Step Case

Figure 7 shows the transient response of the injector opening, the anode pressure, and the ejector manifold to stepped current changes under different control methods. The operating point of the fuel cell stack current is 200 A, and the current stepped up to 300 A instantaneously after 10 s. Considering the operating conditions of the 80 kW fuel cell stack, the desired anode pressure should be maintained at 1.5 bar. The sudden increase in fuel cell current consumed a significant amount of hydrogen in the anode channel, decreasing the anode pressure. The fuel cell stack would suffer hydrogen starvation without a sufficient and timely hydrogen supply. The developed FLC regulated the opening degree of the injector valve, allowing more hydrogen to be fed into the supply manifold. The high pressure at the supply manifold forced more primary flow at the ejector, adding sufficient hydrogen into the anode channel. On the other hand, the fast decrease in the opening degree of the injector valve stabilized the pressure. Continuous hydrogen over-feeding can stack up the anode pressure, leading to an imbalance between the anode and cathode sides. The FLC can decrease the opening degree extremely quickly. As shown in Figure 7b, the FLC can quickly adjust the injector valve opening to 100% and return to a steady state more quickly. As shown in Figure 7c, the FLC can stabilize the anode pressure in less than one second, compared to the two-second stabilization time performance by the conventional PID method. Furthermore, the traditional PID reached an overshoot of anode pressure at 0.41 bar, while the maximum overshoot of anode pressure by the FLC method was only 0.23 bar. The minimum anode pressure regulated by FLC was 1.23 bar, while the anode pressure controlled by traditional PID reached as low as 1.09 bar. The anode pressure fluctuation under the fuzzy logic controller was reduced by about 6.7% compared to the PID control when the current was stepped from 200 A to 300 A. In Figure 7d, FLC also took

less than one second to stabilize the manifold pressure, while the conventional PID method took about 1.3 s. The maximum overshoot under conventional PID regulation was about 0.08 bar, while the maximum overshoot under FLC regulation was slightly higher than that of PID, at about 0.1 bar.

3.2. Performance under Dynamic Case

The operating current of the fuel cell stack varies between 200 A and 300 A with a variation of 10 A and a time interval of 5 s. This condition is intended to simulate the transient responses of the injector valve opening, fuel cell anode pressure, and ejector supply manifold pressure when the fuel cell vehicle undergoes continual acceleration and deceleration. As shown in Figure 8b, when the anode stack current was continually decreased or increased, the injector valve opening under FLC regulation was larger, and the responses were all faster. In Figure 8c, FLC took about 0.8 s to stabilize the anode pressure compared with the stabilization time of one second for the conventional PID method. In addition, the anode pressure overshoot of the conventional PID reached 0.08 bar, while the maximum overshoot of the FLC method was only 0.05 bar. The anode pressure fluctuation of the FLC was about 2% lower than that of the PID control. In Figure 8d, the FLC also stabilized the manifold pressure in less than one second, while the conventional PID method took about 1.1 s. The maximum overshoot under both controller adjustments was very close, about 0.01 bar.

4. Discussion

This research establishes a hydrogen supply system model based on a novel ejector modeling method. To ensure the steady operating pressure of the PEMFC during a dynamic transition pattern, this research develops a FLC. The controller shows better performance when the PEMFC current is varied. The fuzzy controller automatically adjusts the PID parameters when the PEMFC systems' parameters change. This makes FLC perform better when facing a nonlinear system. Finally, the effectiveness of the FLC is verified based on a comparative study of PID controllers. This work provides ideas for intelligent control of the PEMFC for better performance and more extended durability. The novel modeling method supports the hydrogen supply system modeling and control. Yet, the cathode supply system is not included. Future work will formulate both the hydrogen and air supply systems. More advanced control methods will be implemented.

5. Conclusions

This paper proposes a new ejector modeling method, based on which an 80 kw PEMFC system is modeled, and a fuzzy logic controller is designed. The operating conditions of the fuel cell vehicle are simulated by changing the current, and the effectiveness of the fuzzy logic controller is verified by comparing it with the PID controller. The simulation results and detailed analysis provide several conclusions.

(1) The proposed ejector modeling method effectively simulates and predicts the ejector performance under various conditions. The imaginary pressure difference at the A-A section supports the novel modeling and enables accurate control-oriented modeling.
(2) The fuzzy PID controller we developed ameliorates the anode pressure error under transient patterns. The maximum pressure difference is bounded by 5% at transient operating patterns.

In summary, the novel modeling method supports the modeling and control of the hydrogen supply system. However, the cathode supply system is not included. Future work will formulate the hydrogen and air supply systems, and a more advanced control method will be implemented.

Author Contributions: Conceptualization, Y.F.; methodology, Z.X.; software, Z.X.; validation, Z.X.; formal analysis, Z.X.; resources, B.L. and Y.T.; writing—original draft preparation, Z.X.; writing—

review and editing, Y.F.; supervision, Z.D. and Y.F.; project administration, B.L.; funding acquisition, B.L. All authors have read and agreed to the published version of the manuscript.

Funding: This research was funded by [National Key Research and Development Program of China] grant number [2022YFB2503504].

Data Availability Statement: Data available on request.

Acknowledgments: We gratefully acknowledge financial support from the National Key Research and Development Program of China (2022YFB2503504).

Conflicts of Interest: The authors declare no conflict of interest.

References

1. Ding, H.; Dong, Y.; Zhang, Y.; Yang, Y.; Wen, C. Energy efficiency assessment of hydrogen recirculation ejectors for proton exchange membrane fuel cell (PEMFC) system. *Appl. Energy* **2023**, *346*, 121357. [CrossRef]
2. He, Y.; Zhou, Y.; Yuan, J.; Liu, Z.; Wang, Z.; Zhang, G. Transformation towards a carbon-neutral residential community with hydrogen economy and advanced energy management strategies. *Energy Convers. Manag.* **2021**, *249*, 114834. [CrossRef]
3. Daud, W.R.W.; Rosli, R.E.; Majlan, E.H.; Hamid, S.A.A.; Mohamed, R.; Husaini, T. PEM fuel cell system control: A review. *Renew. Energy* **2017**, *113*, 620–638. [CrossRef]
4. Gao, X.; Chen, J.; Xu, R.; Zhen, Z.; Zeng, X.; Chen, X.; Cui, L. Research progress and prospect of the materials of bipolar plates for proton exchange membrane fuel cells (PEMFCs). *Int. J. Hydrogen Energy* **2023**, *50*, 711–743. [CrossRef]
5. Lee, H.Y.; Su, H.C.; Chen, Y.S. A gas management strategy for anode recirculation in a proton exchange membrane fuel cell. *Int. J. Hydrogen Energy* **2018**, *43*, 3803–3808. [CrossRef]
6. Song, Y.; Wang, L.; Jia, L.; Wang, X. Optimization and performance investigation of confocal twin-nozzle ejector for PEMFC hydrogen supply and recirculation system under actual variable operating conditions. *Int. J. Hydrogen Energy* **2023**, *50*, 1450–1464. [CrossRef]
7. Aminudin, M.A.; Kamarudin, S.K.; Lim, B.H.; Majilan, E.H.; Masdar, M.S.; Shaari, N. An overview: Current progress on hydrogen fuel cell vehicles. *Int. J. Hydrogen Energy* **2023**, *48*, 4371–4388. [CrossRef]
8. Huang, P.H.; Kuo, J.K.; Wu, C.B. Design and evaluation of dual passive hydrogen recovery subsystem for 10 kW PEMFC. *Int. J. Hydrogen Energy* **2023**, *54*, 483–490. [CrossRef]
9. Wang, X.; Zheng, J.; Hao, Z.; Di, Y.; Miao, X. Study on the effect of pulsed gas flow on the entrainment performance of hydrogen ejector. *Int. J. Hydrogen Energy* **2024**, *67*, 599–607. [CrossRef]
10. Yuan, H.; Dai, H.; Wu, W.; Xie, J.; Shen, J.; Wei, X. A fuzzy logic PI control with feedforward compensation for hydrogen pressure in vehicular fuel cell system. *Int. J. Hydrogen Energy* **2021**, *46*, 5714–5728. [CrossRef]
11. Zhu, Y.; Cai, W.; Wen, C.; Li, Y. Shock circle model for ejector performance evaluation. *Energy Convers. Manag.* **2007**, *48*, 2533–2541. [CrossRef]
12. Dadvar, M.; Afshari, E. Analysis of design parameters in anodic recirculation system based on ejector technology for PEM fuel cells: A new approach in designing. *Int. J. Hydrogen Energy* **2014**, *39*, 12061–12073. [CrossRef]
13. Wang, X.; Xu, S.; Xing, C. Numerical and experimental investigation on an ejector designed for an 80 kW polymer electrolyte membrane fuel cell stack. *J. Power Sources* **2019**, *415*, 25–32. [CrossRef]
14. Huang, B.J.; Chang, J.M.; Wang, C.P.; Petrenko, V.A. A 1-D analysis of ejector performance. *Int. J. Refrig.* **1999**, *22*, 354–364. [CrossRef]
15. Nikiforow, K.; Koski, P.; Karimäki, H.; Ihonen, J.; Alopaeus, V. Designing a hydrogen gas ejector for 5 kW stationary PEMFC system–CFD-modeling and experimental validation. *Int. J. Hydrogen Energy* **2016**, *41*, 14952–14970. [CrossRef]
16. Chen, L.; Xu, K.; Yang, Z.; Yan, Z.; Zhai, C.; Dong, Z. Optimal design of a novel nested-nozzle ejector for PEMFC's hydrogen supply and recirculation system. *Int. J. Hydrogen Energy* **2023**, *48*, 27330–27343. [CrossRef]
17. Han, J.; Zhao, B.; Pang, Z.; Feng, J.; Peng, X. Transient characteristics investigation of the integrated ejector-driven hydrogen recirculation by multi-component CFD simulation. *Int. J. Hydrogen Energy* **2022**, *47*, 29053–29068. [CrossRef]
18. He, J.; Choe, S.Y.; Hong, C.O. Modeling and controls of a fuel delivery system with dual recirculation lines for a PEM fuel cell system. In Proceedings of the International Conference on Fuel Cell Science, Engineering and Technology, Denver, CO, USA, 16–18 June 2008; Volume 43181, pp. 661–673.
19. He, J.; Choe, S.Y. Modeling and Control of a Hybrid Fuel Delivery System Based on a Two-Phase Anodic Model of a PEM Fuel Cell. In Proceedings of the International Conference on Fuel Cell Science, Engineering and Technology, Brooklyn, NY, USA, 14–16 June 2010; Volume 44045, pp. 771–781.
20. Wang, F.C.; Ko, C.C. Multivariable robust PID control for a PEMFC system. *Int. J. Hydrogen Energy* **2010**, *35*, 10437–10445. [CrossRef]
21. Xue, H.; Zhang, H.; Sun, W.; Yao, A.; Jia, L. An optimized Fuzzy PI control method utilizing an improved QPSO for the hydrogen supply of PEMFC. In Proceedings of the 2023 IEEE 18th Conference on Industrial Electronics and Applications (ICIEA), Ningbo, China, 18–22 August 2023; pp. 603–608.

22. Wang, Y.; Zhang, H.; He, S.; Wang, W.; Gao, M.; Moiseevna, K.E.; Anatolievna, V.V. Dynamic analysis and control optimization of hydrogen supply for the proton exchange membrane fuel cell and metal hydride coupling system with a hydrogen buffer tank. *Energy Convers. Manag.* **2023**, *291*, 117339. [CrossRef]
23. Li, C.; Li, X.; Jiang, W. Model-based control strategy research for the hydrogen system of fuel cell. *IFAC-PapersOnLine* **2021**, *54*, 67–71. [CrossRef]
24. Huang, Y.; Jiang, P.; Zhu, Y. Quasi-two-dimensional ejector model for anode gas recirculation fuel cell systems. *Energy Convers. Manag.* **2022**, *262*, 115674. [CrossRef]
25. Shao, Y.; Xu, L.; Fang, C.; Li, J.; Xu, L.; Hu, Z.; Shi, L.; Ouyang, M. Adoptive Control of Injector for Polymer Electrolyte Membrane Fuel Cell Hydrogen Feeding System. In Proceedings of the 2021 IEEE 4th International Electrical and Energy Conference (CIEEC), Wuhan, China, 28–30 May 2021; pp. 1–6.
26. Pei, P.; Ren, P.; Li, Y.; Wu, Z.; Chen, D.; Huang, S.; Jia, X. Numerical studies on wide-operating-range ejector based on anodic pressure drop characteristics in proton exchange membrane fuel cell system. *Appl. Energy* **2019**, *235*, 729–738. [CrossRef]
27. Kuo, J.K.; Thamma, U.; Wongcharoen, A.; Chang, Y.K. Optimized fuzzy proportional integral controller for improving output power stability of active hydrogen recovery 10-kW PEM fuel cell system. *Int. J. Hydrogen Energy* **2023**, *50*, 1080–1093. [CrossRef]
28. Baroud, Z.; Benmiloud, M.; Benalia, A.; Ocampo-Martinez, C. Novel hybrid fuzzy-PID control scheme for air supply in PEM fuel-cell-based systems. *Int. J. Hydrogen Energy* **2017**, *42*, 10435–10447. [CrossRef]
29. Yang, F.; Li, Y.; Chen, D.; Hu, S.; Xu, X. Evaluation method of oxygen excess ratio control under typical control laws for proton exchange membrane fuel cells. *Int. J. Hydrogen Energy* **2023**, *48*, 28516–28527. [CrossRef]
30. Benchouia, N.E.; Derghal, A.; Mahmah, B.; Madi, B.; Khochemane, L.; Aoul, E.H. An adaptive fuzzy logic controller (AFLC) for PEMFC fuel cell. *Int. J. Hydrogen Energy* **2015**, *40*, 13806–13819. [CrossRef]